Kinetic and Spectroscopic Study of $^1O_2$ Generation from H_2O_2 Catalyzed by LDH – MoO_4^{2-} (LDH = Layered Double Hydroxide)

Bert F. Sels, Dirk E. De Vos, Piet J. Grobet, and Pierre A. Jacobs*[a]

Abstract: Layered double hydroxides (LDHs), exchanged with molybdate, decompose H_2O_2 to form one molecule of singlet-state dioxygen ($^1O_2$) from two molecules of H_2O_2. The dependence of the kinetics of H_2O_2 decomposition on Mo and H_2O_2 concentrations and on temperature has been related to structural characteristics of the material (X-ray diffraction (XRD), scanning electron microscopy (SEM), IR spectroscopy, N_2 adsorption, thermogravimetry) and to molybdate speciation as revealed by in-situ studies in the presence of peroxide (FT Raman, diffuse reflectance UV/visible spectroscopy). The H_2O_2 decomposition rate is linearly correlated with the amount of LDH-exchanged molybdate, except when a considerable fraction of the molybdate occupies less accessible interlayer positions. A maximum in the H_2O_2 decomposition rate as the H_2O_2 concentration is increased is due to the successive formation of mono-, di-, tri-, and tetraperoxomolybdates. This behavior was modeled successfully by using the equilibrium constants for formation of the Mo – peroxo complexes, and the rate constants for decay of the peroxomolybdates with $^1O_2$ liberation. Time-resolved diffuse reflectance and Raman observations of the various MoO_4^{2-} – peroxide adducts are in line with the proposed kinetic scheme. Of all the Mo – peroxo species on the LDH, the triperoxomolybdate has the highest rate for decay to $^1O_2$. Comparison with the kinetics of dissolved molybdate shows that the monomolecular decay of all peroxomolybdate species proceeds much faster at the LDH surface than in solution. Consequently, maximal rates per Mo atom are at least twice as high for the heterogeneous LDH catalyst as for the homogeneous systems.

Keywords: hydrogen peroxide · kinetics · layered compounds · molybdenum · singlet oxygen

Introduction

The first paper on the catalytic decomposition of H_2O_2 by MoO_4^{2-} appeared in 1927,[1, 2] but only recently was the spin multiplicity of the released oxygen studied in more detail. It is now clear that singlet molecular oxygen ($^1O_2$) is generated in the presence of catalytic amounts of MoO_4^{2-}.[3] Moreover, it has been shown that $^1O_2$ is formed quantitatively from the H_2O_2 [Eq. (1)].[4]

$$2\,H_2O_2 \xrightarrow{MoO_4^{2-}} 2\,H_2O + O_2\,(^1\Delta_g) \qquad (1)$$

As $^1O_2$ is evolved upon gentle heating of isolated peroxomolybdate complexes, peroxomolybdate intermediates are the direct precursors to $^1O_2$.[5] Early kinetic results suggested that in aqueous solutions the diperoxomolybdate $MoO_2(O_2)_2^{2-}$ was the main precursor to $^1O_2$, whereas the tetraperoxomolybdate $Mo(O_2)_4^{2-}$ seemed inactive.[4, 6] However, this picture was later modified and refined by coupling kinetic data and spectroscopic experiments. Whereas Raman, IR, and UV/Vis spectroscopy failed to distinguish unequivocally among the various peroxomolybdates,[7, 8] several peroxomolybdates (such as mono-, di-, tri-, and tetraperoxomolybdate) were identified unambiguously by ^{95}Mo NMR spectroscopy.[9] Comparison of the ^{95}Mo NMR data with the kinetics of H_2O_2 decomposition led to the conclusion that triperoxomolybdate $MoO(O_2)_3^{2-}$ is the main precursor of $^1O_2$, while the other peroxomolybdates $MoO_3(O_2)^{2-}$, $MoO_2(O_2)_2^{2-}$, and $Mo(O_2)_4^{2-}$ do not contribute significantly to the formation of $^1O_2$. Therefore, for efficient and rapid $^1O_2$ generation, the experimental conditions, such as pH and the Mo:H_2O_2 molar ratio, must be chosen carefully in order to maximize the triperoxomolybdate concentration. Optimum conditions can be derived from speciation diagrams (pH versus $\log[H_2O_2]_0$) of the various peroxomolybdate intermediates.[10]

As $^1O_2$ is a valuable reagent in organic chemistry,[11] the MoO_4^{2-}/H_2O_2 catalytic system offers an attractive alternative to, as examples, the Kasha – Khan reaction between NaOCl and H_2O_2 or the photosensitized generation of $^1O_2$.[12, 13] In this respect, the MoO_4^{2-}/H_2O_2 system has been found satisfactory for the dioxygenation of unsaturated hydrocarbons, especially in aqueous conditions as in the synthesis of

[a] Prof. P. A. Jacobs, Dr. B. F. Sels, Dr. D. E. De Vos, Prof. P. J. Grobet
Centre for Surface Chemistry and Catalysis
Katholieke Universiteit Leuven
Kardinaal Mercierlaan 92, 3001 Heverlee (Belgium)
Fax: (+32) 16-32-1998
E-mail: pierre.jacobs@agr.kuleuven.ac.be

  0947-6539/01/0712-2547 $ 17.50+.50/0

endoperoxides and dienone hydroperoxides.[14, 15] However, since MoO_4^{2-} and the NaOH which is required for pH control are scarcely soluble even in common organic solvents, this system has its limitations in apolar organic solvents. To overcome this incompatibility, Aubry and co-workers proposed the use of microemulsions, in which $^1O_2$ is formed in the aqueous droplets and diffuses into the organic solvent.[16, 17]

Alternatively, heterogenization of the MoO_4^{2-} catalyst makes it applicable in organic media. Traditional polystyrene resins have been used successfully as anion exchangers for molybdate immobilization.[18] However, in view of the thermal and oxidative stability of the catalyst, immobilization on inorganic materials such as layered double hydroxides (LDHs) is preferable. For example, we have demonstrated that MoO_4^{2-} exchanged on LDH promotes the decomposition of H_2O_2 with selective formation of $^1O_2$.[19, 20] For application of this heterogeneous $^1O_2$ generator to organic synthesis, optimization of its performance is a prerequisite.

We therefore report here on a detailed study of the chemical kinetics of H_2O_2 decomposition in the presence of MoO_4^{2-}-exchanged LDHs. The relationship between the overall H_2O_2 decomposition rate and empirical parameters such as the concentration of MoO_4^{2-} and H_2O_2 and the reaction temperature is discussed. The kinetic behavior is rationalized in terms of several peroxomolybdate intermediates, for which evidence is obtained from in-situ diffuse reflectance spectroscopy (DRS) and Raman spectroscopic studies.

Results

Characterization of LDH–NO_3^- exchanged with MoO_4^{2-}: The chemical compositions of the LDH–MoO_4^{2-} (LDH = layered double hydroxide) samples (Table 1) analyzed by inductively coupled plasma (ICP) measurements and electron probe micro-analysis (EPM) point to a high degree of homogeneity of the elements throughout the LDH material. The experimental Mg:Al ratio (2.18) for the initial LDH is close to the theoretical value of the starting solution. Since this ratio does not vary significantly upon exchange with MoO_4^{2-} anions, no selective dissolution of Mg or Al takes place during the anion exchange process. Mo:Al ratios in the exchange suspension and in the eventual material are compared in Figure 1. At low levels of MoO_4^{2-} the slope of

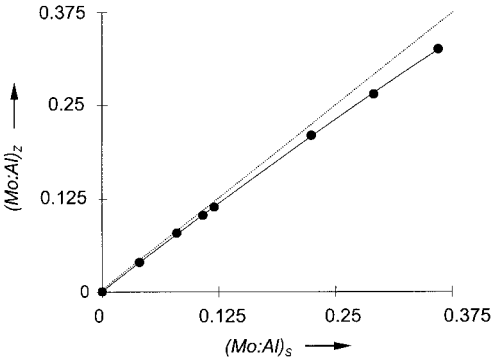

Figure 1. Uptake of MoO_4^{2-} by LDH–NO_3^- samples from aqueous molybdate solutions (25 °C, 12 h under N_2; for further conditions see Experimental Section). $(Mo:Al)_S$ and $(Mo:Al)_Z$ are the molar Mo:Al ratios in the starting exchange slurry and in the eventual powder, respectively.

the isotherm is unity, which indicates a complete uptake of MoO_4^{2-}. Only at higher levels of Mo does the uptake of MoO_4^{2-} level off slightly. This exchange behavior is in agreement with the higher affinity of LDHs for dianionic MoO_4^{2-} than for monoanionic NO_3^-.[23]

Clearly all LDH–MoO_4^{2-} samples show the characteristic X-ray powder pattern of the LDH structure, with lines at 8.2–8.4 Å (003), 4.1–4.2 Å (006), and 1.52 Å (110) (Figure 2).[24] As more MoO_4^{2-} is taken up by the material no new peaks appear, an indication that new phases, such as insoluble $MgMoO_4$, are not formed. Moreover, as the diffraction peaks show only marginal shifts, there is no evidence for phase segregation between nitrate- and molybdate-exchanged LDH. The c_0 and a_0 cell dimensions are collected in Table 1. For completely molybdate-exchanged LDHs, the height of the basal space would be around 9 Å,[25] which is considerably greater than was observed here. At Mo:Al < 0.08 there is no discernible change in the intensity of the first basal (003) peak (Figure 3), but thereafter the intensity clearly decreases with increasing Mo:Al. These data can be interpreted in terms of anion siting during the exchange process. At low Mo loading

Table 1. Chemical analysis, cell dimensions, porosity, and thermal analysis of LDH–NO_3^- and LDH–MoO_4^{2-} samples.

		ICP analysis [mol mol^{-1}]		EPM analysis [mol mol^{-1}]		Weight loss [wt.%]		BET surface	Mesopore	Cell dimension [Å]	
Sample	Mo:Al	Mg:Al	Mo:Al	Mg:Al	Mo:Al (±SD)[a]	below 270 °C	above 270 °C	area [m^{2}g^{-1}]	volume [mL g^{-1}]	a_0	c_0
A LDH–NO_3^-	–	2.18	–	2.18	–	11.8 (<190 °C)[b]	34.6	–	–	–	–
B LDH–MoO_4^{2-}	0.000[c]	2.16	–	2.20	–	12.6 (<190 °C)	33.9	89	0.90	1.523	8.425
C LDH–MoO_4^{2-}	0.040	2.16	0.039	2.21	0.038 ± 0.003	12.7 (<212 °C)	32.3	–	–	1.523	8.382
D LDH–MoO_4^{2-}	0.056	–	–	2.18	0.056 ± 0.005	–	–	87	0.88	1.523	8.359
E LDH–MoO_4^{2-}	0.080	2.15	0.078	2.22	0.077 ± 0.008	12.7 (<217 °C)	29.6	–	–	1.523	8.305
F LDH–MoO_4^{2-}	0.108	2.14	0.103	2.23	0.10 ± 0.01	–	–	–	–	–	–
G LDH–MoO_4^{2-}	0.120	2.15	0.114	2.21	0.12 ± 0.01	13.1 (<220 °C)	29.0	–	–	1.523	8.262
H LDH–MoO_4^{2-}	0.161	–	–	2.21	0.15 ± 0.01	13.5 (<223 °C)	27.5	–	–	1.525	8.262
I LDH–MoO_4^{2-}	0.224	2.13	0.199	2.24	0.20 ± 0.01	13.6 (<235 °C)	24.0	–	–	1.523	8.211
J LDH–MoO_4^{2-}	0.291	2.15	0.265	2.24	0.27 ± 0.01	13.9 (<236 °C)	21.6	–	–	1.523	8.242
K LDH–MoO_4^{2-}	0.358	2.15	0.325	2.22	0.33 ± 0.02	14.0 (<238 °C)	20.3	70	0.56	1.523	8.623[d]

[a] The standard deviation (SD) was obtained from 30 independent analyses. [b] Lowest temperature at which the dehydration process was complete. [c] Sample **B** underwent the same anion exchange procedure in the absence of the molybdate salt. [d] Very broad diffraction peak (see Figure 2).

0947-6539/01/0712-2548 $ 17.50+.50/0 *Chem. Eur. J.* **2001**, *7*, No. 12

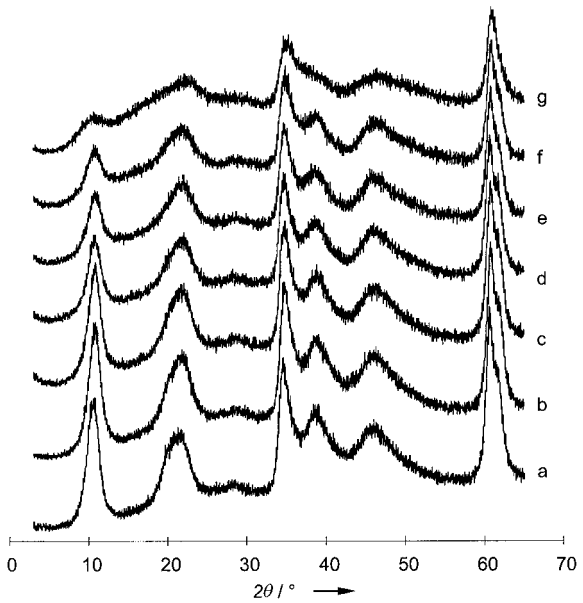

Figure 2. Powder XRD patterns for LDH samples with increasing MoO_4^{2-} content (see Table 1 for sample descriptions): a) **B**; b) **E**; c) **G**; d) **H**; e) **I**; f) **J**; g) **K**.

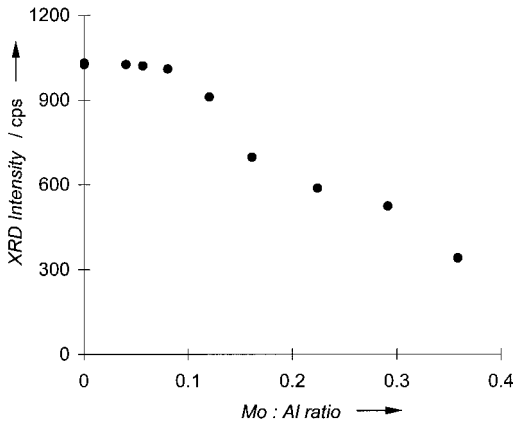

Figure 3. XRD intensity of the first basal peak ($2\theta \approx 10°$) for MoO_4^{2-}-exchanged LDH–NO_3^- as a function of the Mo content.

only NO_3^- in close contact with the exchange solution (for example, at the outer surface and edges) will be exchanged, whereas at higher Mo loadings MoO_4^{2-} will enter the interlayer of the LDH. Since no new phase was detected clearly in the X-ray diffraction (XRD) patterns, the intercalation must proceed inhomogeneously by local structural distortion of the layers, resulting in an irregular stacking of the individual layers within the crystal structure. Since a_0, which is related to the mean cationic radius within the cationic layers and is a direct measure of the Mg:Al atomic ratio in these layers, remains unchanged for all samples (Table 1), it is concluded that the anion exchange process causes no significant change in the chemical composition of the cationic hydroxide layers themselves, in agreement with the chemical analysis.

Scanning electron micrographs were recorded for the various LDH–MoO_4^{2-} samples. As an example, in Figure 4 the **K** sample is seen as particles of agglomerated flat crystallites, with an average diameter of less than 200 nm

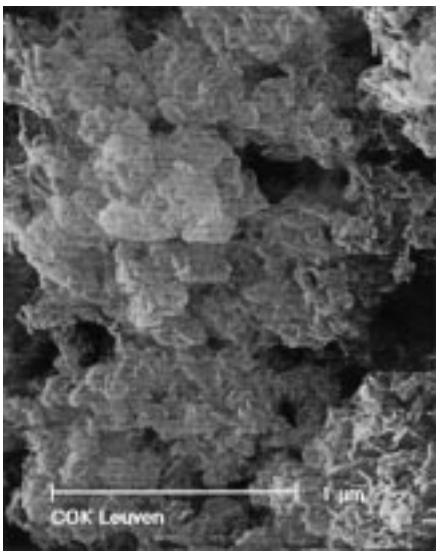

Figure 4. Scanning electron micrograph of **K**.

and a height of 15–25 nm. No clear relationship between, for example, particle size or morphology and Mo loading can be derived from the scanning electron microscope (SEM) pictures.

Nitrogen sorption experiments on LDH–MoO_4^{2-} after outgassing at 125 °C for 4 h (Table 1) showed that: 1) the BET surface decreases with increasing Mo content; 2) the samples do not possess any microporosity; 3) the total mesopore volume decreases with increasing Mo content; and 4) the pore size distribution is most uniform for samples with a high Mo content, with a maximum at pore radii of 3–7 nm. Therefore, the exchange with MoO_4^{2-} causes an aggregration of the small LDH particles, even if the resolution of the SEM experiment is insufficient to confirm this visually. Such flocculation is in agreement with the higher charge of molybdate than nitrate. The dianionic molybdate compensates the electrostatic repulsion between individual LDH crystallites more effectively and therefore facilitates contact that leads to aggregation. In addition, the results of the N_2 sorption experiments are consistent with the empirical observation that the powder samples with the highest MoO_4^{2-} loading showed the highest volume density.

The results of thermogravimetric analyses and the corresponding DTG profiles (Figures 5 and 6, respectively) for selected samples are summarized in Table 1. The amount of surface and interlayer water, derived from the weight loss below approximately 270 °C, tends to grow with increasing MoO_4^{2-} loading. The DTG curve for the original LDH–NO_3^- (**A**) shows a single maximum at 115 °C, whereas for the LDH–MoO_4^{2-} samples a clear second maximum appears around 180 °C. The weight loss associated with this maximum increases with the Mo content. Hence, it is clear that because MoO_4^{2-} is present, some of the water molecules are more strongly retained by the structure. Such a bimodal dehydration process has been reported for CO_3^{2-}-intercalated LDHs and was ascribed to the distinct elimination of loosely bound surface water and strongly held interlayer water.[24] Moreover, the intercalation of one MoO_4^{2-} anion instead of two NO_3^-

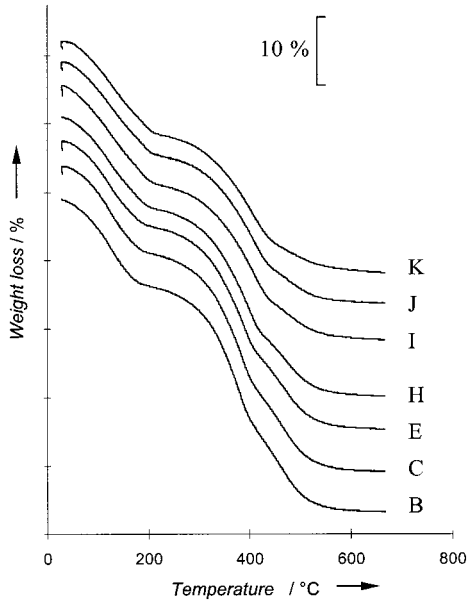

Figure 5. TG curves of the original LDH–NO_3^- (**B**) and molybdate-containing LDHs. Molybdate content increases from bottom to top (see Table 1).

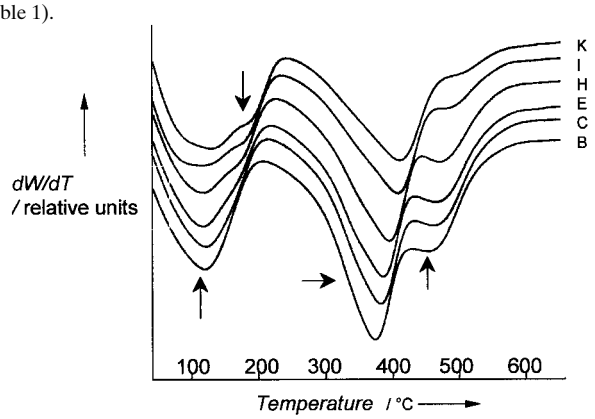

Figure 6. DTG curves for the starting host material (**B**) and for MoO_4^{2-}–LDHs (see Table 1).

anions creates extra space in the interlayer, which can be filled with water molecules. A similar observation was also made for LDH–Cl^- samples that were exchanged with phosphate.[26]

The weight loss between 270 and 650 °C corresponds to dehydroxylation and NO_3^- decomposition. Indeed, the DTG curve for LDH–NO_3^- (**A**) shows two distinct peaks around 385 and 460 °C. As expected, the total weight loss above 270 °C decreases with an increase in the MoO_4^{2-} loading (see Table 1). In particular, the weight loss above 410 °C, that is, above the inflection point in the TG curves, decreases gradually with increasing Mo content and, therefore, may be assigned to the elimination of NO_3^-. Thermal decomposition experiments have demonstrated that NO_3^- anions exchanged on NiMgAl–LDHs are decomposed at temperatures ranging from 380 to 420 °C.[27] The dehydroxylation clearly shifts to higher temperatures (from 385 to 410 °C) with increasing Mo loading, probably because of stronger interactions of the dianionic MoO_4^{2-} with the brucite-type sheets.

The single resonance observed around $\delta = 9$ in the ^{27}Al MAS-NMR spectra of LDH–MoO_4^{2-} samples **B**, **C**, and **K** (Figure 7) is indicative of the octahedral coordination of Al.[28]

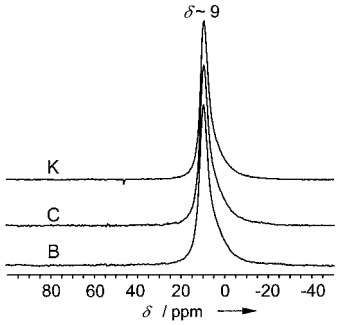

Figure 7. ^{27}Al NMR spectra of LDH–MoO_4^{2-} samples **B**, **C**, and **K** (see Table 1).

Since no signal intensity was observed around $\delta = 60$, the samples are free of tetrahedrally coordinated Al. The ^{27}Al spectra of the two MoO_4^{2-}-exchanged LDHs **C** and **K** are identical to that of the starting LDH–NO_3^- (**B**). Thus, the replacement of NO_3^- with MoO_4^{2-} does not influence the chemical status of Al, suggesting the occurrence of a topotactic anion exchange process.

The IR spectrum for the LDH without MoO_4^{2-} (**B**) between 500 and 1900 cm^{-1} (Figure 8) shows a broad absorption band at 3472 cm^{-1} with a shoulder at 3565 cm^{-1}. These bands are

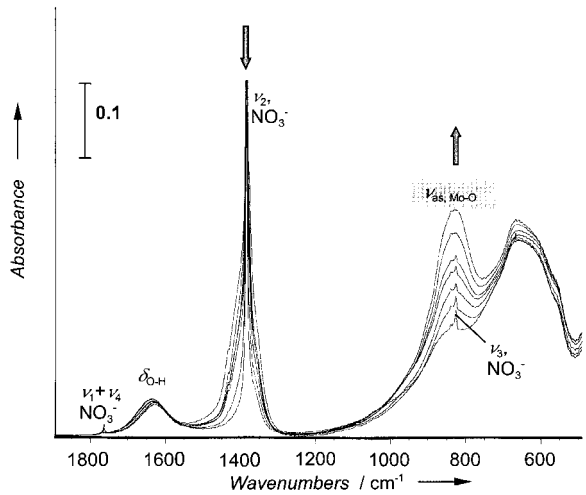

Figure 8. IR spectra of MoO_4^{2-}-exchanged LDH–NO_3^- samples **B**, **E**, **G**, **H**, **I**, **J**, and **K**, as defined in Table 1.

due to ν(O–H) stretching modes of physisorbed and interlayer water and to the structural hydroxide groups. The broad bending vibration δ_{O-H} is at 1627 cm^{-1}. The three clear absorption bands at 827, 1385, and 1768 cm^{-1} are assigned to NO_3^- anions.[29] The absorbance recorded below 750 cm^{-1} is due to lattice vibrations in the LDH framework. Upon exchange with MoO_4^{2-} anions, a new vibration band appears as a shoulder in the O–H stretching vibration region at 3200 cm^{-1} (not shown). Such a shoulder has also been observed for CO_3^{2-}-containing LDHs and has been ascribed to ν(O–H) of interlayer water molecules hydrogen-bonded with the CO_3^{2-} anions.[30] This supports the idea that some water molecules are quite strongly bonded to MoO_4^{2-} in the MoO_4^{2-}-intercalated LDH material, as was implied from the

0947-6539/01/0712-2550 $ 17.50+.50/0 *Chem. Eur. J.* **2001**, *7*, No. 12

thermal analysis. The most characteristic feature in the IR spectra is a broad absorbance around 831 cm^{-1}, which grows at the expense of the bands associated with NO_3^-. Based on the literature, this band is typically assigned to the M=O stretching of a tetrahedrally coordinated Mo species such as MoO_4^{2-}.[29]

In the Raman spectra of LDH–MoO_4^{2-} samples (Figure 9), four distinct bands can be observed. The absorbance at 550 cm^{-1} is a structural vibration in the cationic LDH layers,

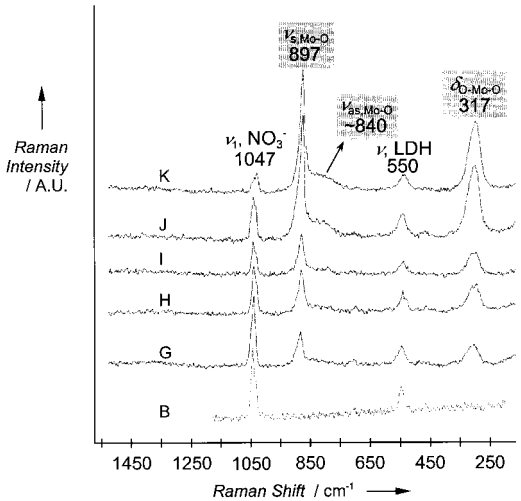

Figure 9. Raman spectra of MoO_4^{2-}-exchanged LDH–NO_3^- samples **B**, **G**, **H**, **I**, **J**, and **K** (see Table 1).

whereas the band centered at 1047 cm^{-1} is the symmetrical stretching vibration ν_1 of NO_3^-. Since the two remaining bands at 897 cm^{-1} (with a shoulder at approximately 840 cm^{-1}) and at 317 cm^{-1} are absent in the LDH–NO_3^- spectrum, and get stronger with increasing Mo content, they can be ascribed to the uptake of Mo. These bands are in diagnostic positions for monomolybdate MoO_4^{2-} with tetrahedral symmetry (T_d).[29] Even for **K**, which has the highest Mo loading (Mo:Al = 0.325) additional peaks, for example, Mo–O–Mo deformation bands near 200 cm^{-1}, were not observed.[31]

Kinetics of H_2O_2 decomposition with LDH–MoO_4^{2-}: A typical evolution of the H_2O_2 concentration, measured by cerimetry, was clearly zero order with respect to H_2O_2 (Figure 10) when hydrogen peroxide (0.29 M) in MeOH was allowed to decompose at 296 K in the presence of LDH–MoO_4^{2-}. The H_2O_2 decomposition rate r_{HP} can be calculated from the slope of the initial linear region. For instance, when **E** reacts with H_2O_2 (0.29 M) in MeOH at 296 K, $r_{HP} = 0.028 \pm 0.002$ mM s^{-1}. Surprisingly, the decomposition rate increases when almost all the H_2O_2 has decomposed.

To investigate the influence of the reaction temperature on r_{HP}, an Arrhenius plot (Figure 11) was obtained for reactions at temperatures ranging from 0 to 30 °C in MeOH, with **E** at 2.5 mM Mo. The initial concentration of H_2O_2 was 0.29 M in all the experiments. The apparent activation energy E_a derived from the slope of Figure 11 was 72.7 ± 6.7 kJ mol^{-1}.

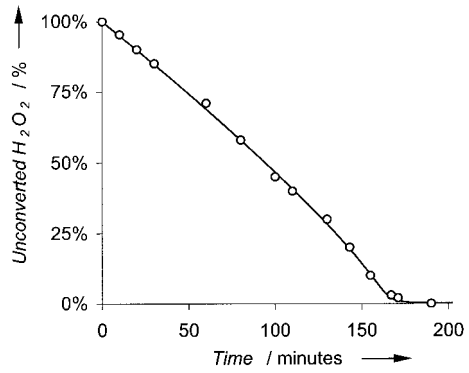

Figure 10. Typical kinetic profile of the decomposition of H_2O_2 (0.29 M) by **E** in MeOH at 296 K by using MoO_4^{2-} (3.6 mM) (○). The full line represents the curve fitting with the K_i and k_i parameters of Table 2 (bottom line).

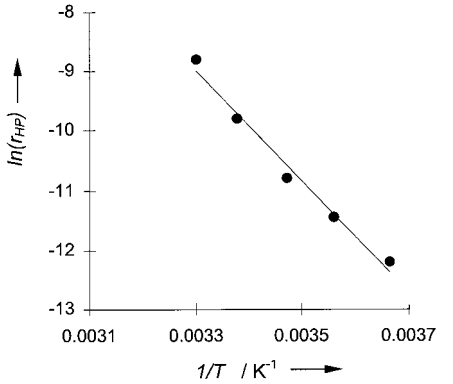

Figure 11. Arrhenius plot for the disappearance of H_2O_2 (0.29 M) in the presence of **E**.

The dependence of r_{HP} on [Mo] at Mo concentrations varying between 1.5 and 16 mM by two procedures (A and B) is summarized in Figure 12. With procedure A, r_{HP} increased

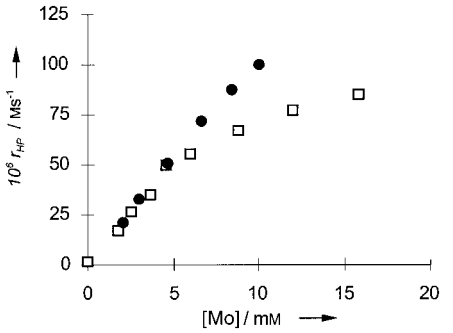

Figure 12. Influence of the amount of catalyst **E** on the decomposition of H_2O_2: by procedure A (●), varying the total weight of catalyst, with constant MoO_4^{2-} loading; and by procedure B (□), changing the degree of MoO_4^{2-} exchange on a constant mass of solid LDH. The initial concentration of H_2O_2 was always 0.29 M, in MeOH at 296 K.

linearly with the amount of catalyst by a first-order reaction in the range 1.8–11 mM. The slope of the plot corresponds to a turnover frequency, that is, an average activity per immobilized MoO_4^{2-} anion, of $(9.8 \pm 0.7) \times 10^{-3}$ s^{-1} (Figure 12). For procedure B there were two distinct stages: at Mo:Al ≤ 0.12 (5 mM Mo in Figure 12), the consumption of H_2O_2 was

proportional to the Mo concentration. The pseudo first-order rate constant obtained was $(10.1 \pm 0.8) \times 10^{-3}\,s^{-1}$, which corresponded within experimental error to the value from procedure A. However, at higher Mo contents r_{HP} leveled off, pointing to a reaction order in Mo of between one and zero.

The influence of the initial hydrogen peroxide concentration $[H_2O_2]_0$ on the H_2O_2 decomposition rate in presence of 1 mM Mo was investigated in MeOH at 296 K, with Na_2MoO_4 and **E** as Mo sources. The dependence of r_{HP} on $[H_2O_2]_0$ up to 0.3 M behaves in a similar, complex manner for both MoO_4^{2-} catalysts (Figure 13). Three clear stages can be distinguished:

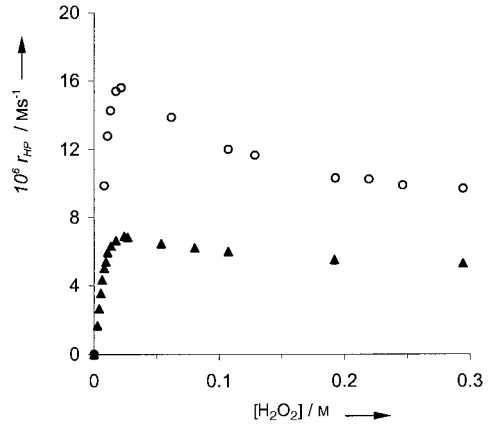

Figure 13. Influence of the initial $[H_2O_2]_o$ on the decomposition rate r_{HP} in the presence of (○) **E**, or (▲) Na_2MoO_4, in NaOH (0.05 M). The total Mo concentration was 1 mM in both cases.

1) a region of steep gradient at low $[H_2O_2]_0$; 2) a well-defined maximum in r_{HP} for intermediate $[H_2O_2]_0$; and 3) an almost constant r_{HP} at high $[H_2O_2]_0$. In the initial phase with Na_2MoO_4 ($[H_2O_2]_0 < 0.008$ M), the reaction is second order in H_2O_2. For the decomposition by LDH–MoO_4^{2-} at $[H_2O_2]_0 < 0.015$ M, the order is between one and two. The maximum decomposition rate with LDH–MoO_4^{2-} (15.7×10^{-6} M s^{-1}) is at 0.021 M $[H_2O_2]_0$, whereas the decomposition rate measured in homogeneous conditions is highest for 0.032 M H_2O_2 with a value of 6.9×10^{-6} M s^{-1}. Over the whole range of $[H_2O_2]_0$, the heterogeneous catalyst decomposes H_2O_2 faster than the homogeneous one.

In-situ spectroscopy of the working catalyst: It is well established that the decomposition of H_2O_2 by MoO_4^{2-} in solutions involves the formation of different peroxomolybdate complexes.[4, 9, 10, 32] An in-situ spectroscopic study was therefore undertaken to obtain insight into the nature of these peroxo intermediates formed at the LDH surface.

To establish reliable correlations with the kinetic data, DRS measurements were realized under the usual catalytic conditions (**E** at 3.6 mM Mo, at 296 K in MeOH). Initially, the suspension of LDH–MoO_4^{2-} in MeOH is white (spectrum not shown). Upon exposure to 0.29 M H_2O_2, the suspension rapidly turns red-brown. In the reflectance spectrum (Figure 14) this color change is accompanied by the appearance of a peak at 450 nm (22200 cm^{-1}). As H_2O_2 is progressively decomposed, this band gradually decreases, while a new band is formed at 330 nm (30300 cm^{-1}). There are two clear

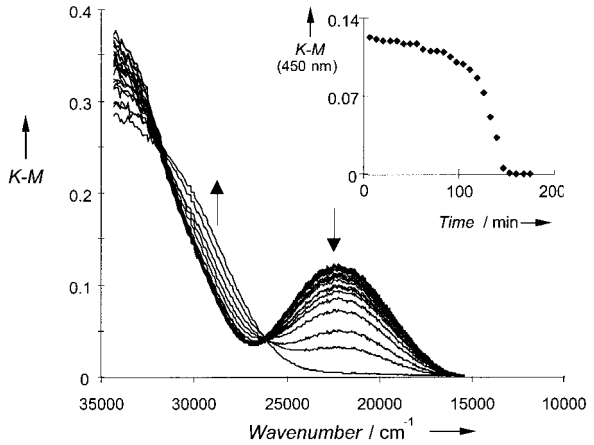

Figure 14. Consecutive time-resolved DR spectra for decomposition of H_2O_2 in the presence of catalyst **E** (3.6 mM Mo) and H_2O_2 (0.29 M) in MeOH at 296 K. Spectra were recorded at 6–7 min time intervals.

isosbestic points, at 380 nm (26300 cm^{-1}) and 310 nm (32300 cm^{-1}), suggesting that the spectrum may originate from two distinct colored species. When the consumption of H_2O_2 is complete, the catalyst turns white again. The Figure 14 inset illustrates the time dependence of the light absorption at 450 nm, expressed as the Kubelka–Munk value. Since the only colored species at 450 nm is the red-brown tetraperoxomolybdate,[7] this curve directly parallels the $Mo(O_2)_4^{2-}$ concentration during the decomposition of H_2O_2. This concentration appears to be practically constant for the larger part of the reaction. The band at 330 nm can be ascribed to the $O_2^{2-} \rightarrow Mo^{VI}$ ligand-to-metal charge transfer (LMCT) of the yellow mono- and diperoxomolybdates (for example, $MoO_3(O_2)^{2-}$, $MoO_2(O_2)_2^{2-}$, $HMoO_2(O_2)_2^{-}$, and $Mo_2O_3(O_2)_4^{2-}$).[7, 9, 32–34]

In-situ Raman measurements were carried out with a suspension of **I** at 30 mM Mo, and 3.3 M H_2O_2 in MeOH. The H_2O_2:Mo molar ratio was maintained in the same range, but the suspension was more concentrated in both $[MoO_4^{2-}]$ and $[H_2O_2]$ than that used in, for example, Figures 10 and 14, so caution must be exercised in establishing relationships with the catalytic data. Figure 15 shows time-resolved Raman spectra recorded during the decomposition of H_2O_2, with the color of the suspension indicated on the right. The absorption bands at 1065 and 1462 cm^{-1} are due to the solvent MeOH,[35] whereas the band at 554 cm^{-1} is typical of the lattice vibrations in the LDH layers.[23b] Clearly, these bands should not change throughout the experiment. In excess H_2O_2, the diagnostic bands of MoO_4^{2-} (898, 841, 317 cm^{-1}) are not observed. However, there are two clear bands at 873 and 527 cm^{-1} (trace a). The former band is probably a superposition of the ν(O–O) vibrations of H_2O_2 and of Mo-coordinated O_2^{2-}. Such bands are normally situated at 872 cm^{-1}, as measured in a blank experiment without LDH–MoO_4^{2-}, and at 865 cm^{-1}, respectively.[8] The 527 cm^{-1} band is the corresponding ν^s[Mo(O$_2$)]. Since there is no absorbance in the typical region for Mo=O stretching vibrations (920–960 cm^{-1}), Raman spectrum a can be assigned to a fully peroxidized tetraperoxo $Mo(O_2)_4^{2-}$ (D_{2d}). The peak position for ν^s[Mo(O$_2$)] differs slightly from that

0947-6539/01/0712-2552 $ 17.50+.50/0 *Chem. Eur. J.* **2001**, *7*, No. 12

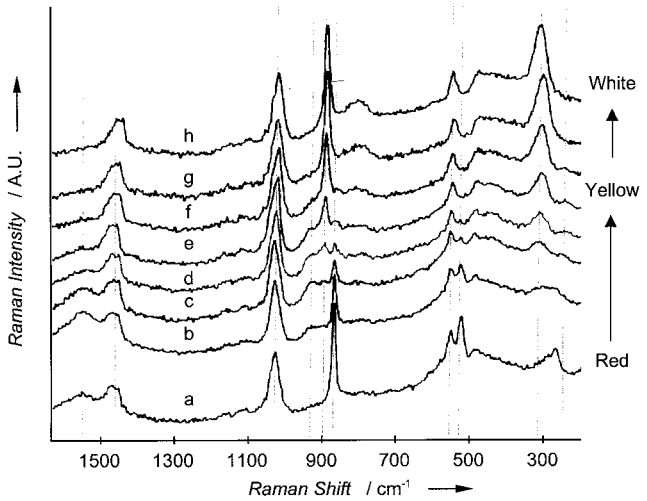

Figure 15. Raman spectra of **I** in MeOH during the decomposition of H_2O_2 (3.3 M) recorded at the following times [min]: a) 20; b) 50; c) 60; d) 70; e) 80; f) 90; g) 130; h) 200.

reported for $(NH_4)_2[Mo(O_2)_4]$.[8] However, we observed an identical Raman spectrum for $K_2[Mo(O_2)_4]$ dissolved in MeOH with excess H_2O_2. Upon consumption of H_2O_2, the color of the suspension changes gradually from red to yellow. The corresponding Raman spectra b–e contain weak bands in the 920–960 cm^{-1} range. These are characteristic stretching vibrations for Mo=O in partially peroxidized molybdate anions (for example, $MoO_3(O_2)^{2-}$, $[MoO_2(O_2)_2^{2-}$, $HMoO_2(O_2)_2^-$, $Mo_2O_3(O_2)_4^{2-}$, $MoO(O_2)_3^{2-}$). The broad Raman bands suggest that several of these species coexist. After complete consumption of H_2O_2, the original spectrum of MoO_4^{2-} is fully restored, as evidenced by the characteristic vibrations at 898, 841, and 317 cm^{-1} (curves f–h). Throughout the decomposition process, there is a band at 1551 cm^{-1}, assigned to the symmetric stretching vibration $\nu_{sym}(O-O)$ of O_2.[29] This confirms that O_2 is formed continuously during the H_2O_2 decomposition.

Discussion

Characterization of the parent molybdate-exchanged LDH: LDH–MoO_4^{2-} materials with various Mo contents have been prepared by a simple anion exchange method. The degree of exchange varied between 0% and 65% of the total anion exchange capacity (AEC), corresponding to Mo:Al ratios between 0 and 0.358. The anion exchange reaction proceeds topotactically; it does not affect the framework of the LDH, as evidenced by elemental analysis, ^{27}Al NMR spectroscopy, and XRD. With low concentrations of MoO_4^{2-}, only NO_3^- anions at the outer surface and near the edges are exchanged, whereas those between the layers are replaced only when the degree of anion exchange is about 20% or more (Figure 3). The intercalation of MoO_4^{2-} causes disordering in the stacking sequence of the individual brucite-like layers and creates extra space, which is filled with water. Despite the two-stage behavior of the exchange, MoO_4^{2-} uptake remains selective for all the MoO_4^{2-} concentrations studied.

Only monomeric MoO_4^{2-} anions were detected on the LDH support, by IR and Raman spectroscopy. No evidence was found for condensation of the molybdate species, for example, by reaction with the Al octahedra of the brucite layer or by oligomerization in the interlayer. Such phenomena are common for phosphate-, silicate-, and vanadate-containing LDHs.[28c, 36] Molybdate may also be intercalated in a polymeric form such as the heptamolybdate anion, $Mo_7O_{24}^{6-}$. However, such intercalation is achieved only when the exchange solution is acidified with an appropriate amount of acid, making the heptamolybdate the dominant species in the exchange solution.[37] Hence, any difference between the LDH–MoO_4^{2-} catalysts in the decomposition of H_2O_2 should be explained in terms of varying accessibility of the MoO_4^{2-} ions, or by changes in the peroxo intermediates that are formed after H_2O_2 exposure; there is no evidence that species other than simple MoO_4^{2-} are present in the system before peroxide addition.

Kinetic model for H_2O_2 decomposition: The kinetic behavior of the peroxo intermediates during the decomposition of H_2O_2 (Scheme 1) includes the formation of several peroxomolybdates from MoO_4^{2-} and H_2O_2, the unimolecular decomposition of the peroxomolybdates into dioxygen and oxomolybdates, the condensation into peroxo dimers, and various acid–base equilibria. The protonation and dimerization reactions may be neglected in view of the basicity of the LDH support.[38] Indeed, the pH of a 1% aqueous suspension of the LDH powder is around 9.5. Thus the large set of possible reactions can be reduced to Equations (2)–(5) in Scheme 1.

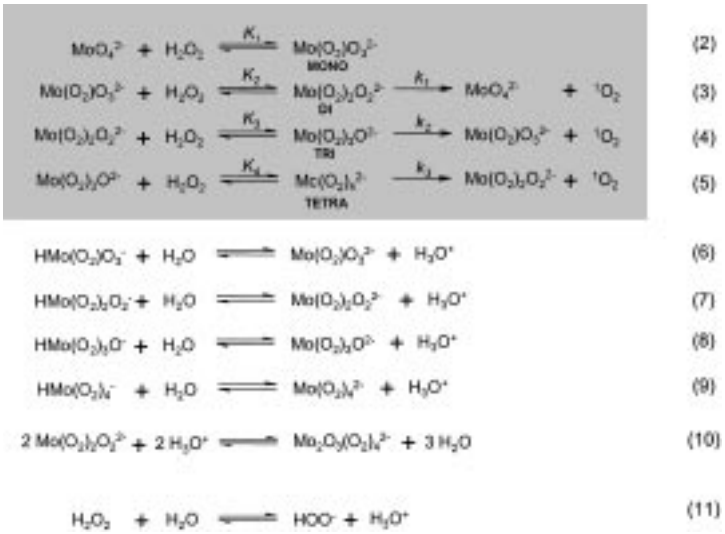

Scheme 1. Formation and reactions of peroxomolybdates. Reactions (2)–(5), in which water molecules are omitted for clarity, are sufficient to model the decomposition of H_2O_2 by LDH–MoO_4^{2-}.

Calculations can be simplified if it is assumed that the equilibration between the metal peroxides and free H_2O_2 is fast compared with their decomposition. Since the steady-state concentration of the highly peroxidized species $Mo(O_2)_4^{2-}$ is attained within minutes (Figure 14, inset), this

condition is fulfilled. Because of the fast equilibria, one can calculate the metal peroxide concentrations by using the equilibrium constants K_1, K_2, K_3, and K_4. Values of these constants for homogeneous equilibria can be found in the literature (Table 2). The simplified kinetics of Scheme 1 (reactions (2) – (5)) lead straightforwardly to Equation (a).

$$r_{HP} = 2\frac{\{k_1 + k_2K_3[H_2O_2] + k_3K_3K_4[H_2O_2]^2\}[Mo_4^{2-}]_0}{\left\{\frac{1}{K_1K_2[H_2O_2]^2} + \frac{1}{K_2[H_2O_2]} + 1 + K_3[H_2O_2] + K_3K_4[H_2O_2]^2\right\}} \quad \text{(a)}$$

Table 2. Equilibrium constants (K_1, K_2, K_3, K_4) and unimolecular rate constants (k_1, k_2, k_3) for formation and decomposition of the Mo – peroxo complexes Compilation of literature values and values obtained in this work.[a]

Reference	K_1	K_2	K_3	K_4	k_1[b]	k_2[b]	k_3[b]
[4][c]	$K_1 \cdot K_2 = 2500$		–	–	4.6	–	–
[6][d]	$K_1 \cdot K_2 = 2500$		–	2.0	4.6	–	0
Fitted with Equation (1)	15	200	230	10	0.2	4.3	1.6
[9, 10][e]	150	1200	210	1.4	0.06	0.6	0
This work:[f]							
Homogeneous[g]	50	1000	300	11	1.5	4.0	2.3
Heterogeneous	20	1500	40	50	5.5	15.5	4.2

[a] Mo concentrations, pH, and solvents may widely differ; this explains some of the discrepancies. [b] Expressed as $\times 10^3\ s^{-1}$. [c] Taking into account only the diperoxomolybdate. [d] Taking into account only the diperoxo- and tetraperoxomolybdate. [e] At 273 K. [f] Fitted with Equation (a). [g] Since at low H_2O_2 concentrations part of the H_2O_2 is deprotonated, the equilibrium constants should be considered as apparent values.

However, no consistent fit of this equation to the set of 51 data points gathered from 1) the dependence of r_{HP} on $[H_2O_2]$ for a reaction catalyzed by LDH-MoO_4^{2-} (Figure 13), 2) the loss of H_2O_2 over time (Figure 10), or 3) the disappearance of $Mo(O_2)_4^{2-}$ as a function of time (Figure 14, inset) was obtained with the K_i values reported for soluble MoO_4^{2-} in H_2O.[4, 6, 9, 10] A parameter set that accounts adequately for the experimental results with LDH – MoO_4^{2-} is given in Table 2. The solid lines in Figure 10 (for r_{HP} versus time) and Figure 16 (for r_{HP} versus $[H_2O_2]$ and Kubelka – Munk value versus time) represent the curves calculated with the aid of the constants from Table 2, and approach the data points within the experimental error.

According to the order for the unimolecular rate constants $k_2 \gg k_1 > k_3$, the decomposition of H_2O_2 to O_2 should proceed most rapidly via the triperoxomolybdate intermediate, $MoO(O_2)_3^{2-}$. LDH-immobilized diperoxomolybdate $MoO_2(O_2)_2^{2-}$ and tetraperoxomolybdate $Mo(O_2)_4^{2-}$ are also involved, but they seem to be three to four times more stable than $MoO(O_2)_3^{2-}$. This agrees well with the reported involvement of the triperoxo complex in H_2O_2 decomposition by the soluble MoO_4^{2-} catalyst.[9, 10] Most interestingly, the propensity of all peroxomolybdates to decompose is more pronounced at the LDH surface than in solution. Indeed, as can be seen from the fitting results (Table 2), the unimolecular decomposition rate constants for the heterogeneous Mo

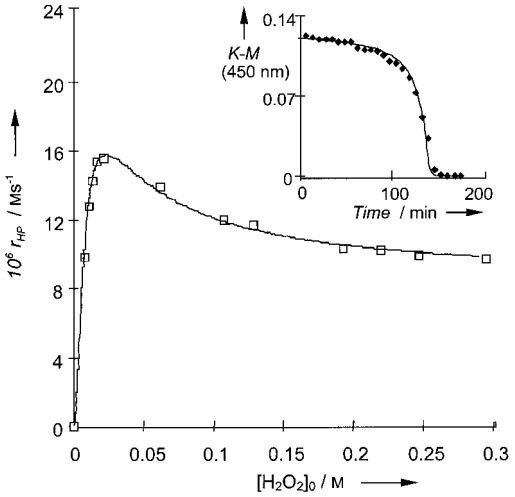

Figure 16. Simulation of the kinetic data with the parameters of Table 2. Influence of the initial $[H_2O_2]_0$ on the decomposition rate r_{HP} in the presence of **E** ($[Mo]_T = 1$ mM). Full line: simulation; □: experimental points (compare Figure 13). Inset: Decay of the 450 nm absorption (expressed as Kubelka – Munk values) as a function of time (see Figure 14). The model predicts the experimental observations with an accuracy better than 5%.

catalyst are higher than those for the soluble peroxomolybdate complexes.

The equilibrium constants K_1, K_2, K_3, and K_4 obtained from the fit can be used to plot the relative fractions of the peroxo species as a function of free $[H_2O_2]$, from which the prevalent species during various stages of the H_2O_2 decomposition process may be predicted (Figure 17). It is apparent from this

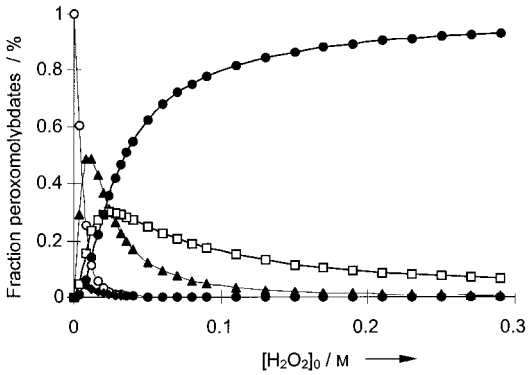

Figure 17. Predicted concentration [%] as a function of $[H_2O_2]_0$ of: ○, MoO_4^{2-}; ◆, $MoO_3(O_2)^{2-}$; ▲, $MoO_2(O_2)_2^{2-}$; □, $Mo_2O(O_2)_3^{2-}$; ●, $Mo(O_2)_4^{2-}$ (296 K, $[Mo] = 3.6$ mM). The equilibrium constants for LDH – MoO_4^{2-} from Table 2 (bottom line) were used.

graph that tetraperoxomolybdate is the main peroxo intermediate at high $[H_2O_2]$, whereas the tri-, di-, and monoperoxomolybdates are involved only at very low $[H_2O_2]$.

Interpretation of the kinetic data: The successive formation of various peroxomolybdate intermediates thus makes it possible to explain the complex kinetics of Figures 10 and 13. Rewriting of Equation (a) makes it clear that the total rate of

0947-6539/01/0712-2554 $ 17.50+.50/0 *Chem. Eur. J.* **2001**, *7*, No. 12

H_2O_2 decomposition, r_{HP}, consists of the sum of separate contributions of di-, tri-, and tetraperoxomolybdates [Eq. (b)].

$$\tfrac{1}{2}r_{HP} = -\frac{1}{2}\frac{d[H_2O_2]}{dt} = k_1[MoO_2(O_2)_2^{2-}] + k_2[MoO(O_2)_3^{2-}] + k_3[Mo(O_2)_4^{2-}] \quad \text{(b)}$$

Figure 17 shows that for fairly high concentrations ($[H_2O_2] > 0.15$ M), the fraction of the various Mo species hardly changes; they comprise mainly $Mo(O_2)_4^{2-}$, with a small amount of $MoO(O_2)_3^{2-}$. According to Equation (b), r_{HP} changes little if the concentrations of the peroxo species are almost constant. Hence, for $[H_2O_2] > 0.15$ M, r_{HP} is independent of the concentration of H_2O_2. This zero-order dependence on H_2O_2 agrees with the initially linear decay of $[H_2O_2]$ in time (Figure 10).

As $[H_2O_2]$ decreases during its decomposition, the overall decomposition rate r_{HP} increases to a maximum value, which can be explained by the formation of less peroxidized intermediates. Indeed, from Figure 17, when $[H_2O_2]$ is decreased triperoxomolybdate becomes the next most abundant species to $Mo(O_2)_4^{2-}$. Since $MoO(O_2)_3^{2-}$ is less stable than $Mo(O_2)_4^{2-}$, r_{HP} becomes higher in this H_2O_2 concentration domain. As the H_2O_2 decomposition continues, the diperoxomolybdate $MoO_2(O_2)_2^{2-}$ becomes an important decomposing agent. Because of the higher stability of $MoO_2(O_2)_2^{2-}$, the H_2O_2 decomposition slows down again, creating a rate maximum (Figure 13). The maximum value corresponds to the optimal combination of the terms in Equation (b).

When almost all the H_2O_2 is consumed, the decomposition becomes very slow. This is ascribed to the very low concentration of the three $^1O_2$ precursors. The monoperoxomolybdate $MoO_3(O_2)^{2-}$ predominates in the suspension, together with MoO_4^{2-} (Figure 17).

The spectroscopic results are consistent with the successive formation of various peroxomolybdates during the H_2O_2 decomposition. Both Raman and diffuse reflectance spectroscopy confirm the prevalence of $Mo(O_2)_4^{2-}$ in H_2O_2-rich conditions, whereas a mixture of lower peroxidized molybdates is observed at low H_2O_2 concentrations. Unfortunately, the spectroscopic techniques are not accurate enough to allow a clear distinction among the partially peroxidized molybdates. Raman spectroscopy did show that all species are completely transformed into MoO_4^{2-} after total consumption of H_2O_2.

The insoluble catalyst LDH–MoO_4^{2-} decomposes H_2O_2 faster than the dissolved MoO_4^{2-} in 0.05 N NaOH. While these conditions might not be the best ones for the dissolved catalyst, it should be noted that in all previous studies with dissolved molybdate, buffers at high pH or simply NaOH have been used.[4, 9, 10] The high values of the unimolecular decomposition rate constants k_2 and k_3 (see Table 2) demonstrate that the tri- and tetraperoxomolybdate anions disproportionate remarkably fast when immobilized on the LDH support. This may be rationalized as follows: the disproportionation of peroxo intermediates proceeds through polarization of the metal–peroxo bonds, Mo–O_2, and the peroxide bonds, O–O, in the peroxomolybdate complex, followed by an inner-sphere two-electron rearrangement.[9, 39] Acceleration of peroxide decomposition on a solid support has been observed previously; the homolytic O–O bond cleavage for alkyl(hydro)peroxides is accelerated in the presence of alkali-exchanged zeolite Y.[40] Similarly, the disproportionation of peroxomolybdate complexes is favored in the vicinity of the highly charged LDH support.

Since a straight line is observed in the Arrhenius plot (Figure 11), it can be assumed that the mechanism of decomposition does not change much in the temperature range 273–303 K. The activation energy for H_2O_2 decomposition by LDH–MoO_4^{2-} (71.2 ± 6.7 kJ mol^{-1}) is close to the 65.2 ± 5.0 kJ mol^{-1} reported by Böhme and Brauer who used dissolved molybdate complexes.[6] The close agreement between homogeneous and heterogeneous E_A values suggests that mass transfer phenomena do not influence the rates, at least not in the initial phase for which rates were measured.

Equation (b) predicts that the decomposition of H_2O_2 by LDH–MoO_4^{2-} is first order with respect to MoO_4^{2-}. This behavior is indeed observed when the amount of LDH catalyst is varied with a constant, low Mo content (Figure 12, ●), and has previously been reported for soluble MoO_4^{2-}.[4, 6] This proportionality relationship between r_{HP} and MoO_4^{2-} is characteristic for a unimolecular disproportionation of the peroxomolybdates, that is, $^1O_2$ originates from two peroxo ligands bonded to the same Mo atom.[9]

However, the order with respect to Mo is between zero and one for H_2O_2 decomposition when the Mo concentration is raised in a fixed amount of LDH (Figure 12, □). This may be explained by a restricted access to the MoO_4^{2-} anions. Indeed, at high loadings of MoO_4^{2-}, some of the MoO_4^{2-} anions are intercalated between the sheets of the LDH, diffusion to these intercalated Mo anions is consequently more difficult, and the overall reaction rate no longer increases proportionally with the overall Mo concentration. On the basis of the XRD data, a similar differentiation between easily accessible and intercalated Mo anions can be expected. The inflection points in Figures 12 and 3 both correspond to approximately 20% occupation of the AEC by MoO_4^{2-}, that is, to Mo:Al = 0.1.

Conclusion

The kinetics of H_2O_2 decomposition in MeOH catalyzed by LDH–MoO_4^{2-} have been examined by cerimetry. The data can be modeled by the successive formation of mono-, di-, tri-, and tetraperoxomolybdates. The triperoxomolybdate is the least stable intermediate. Nevertheless, the tetraperoxomolybdate is the predominating species in H_2O_2-rich conditions. Achievement of a high decomposition rate per mole of Mo has the following requirements: 1) the loading of MoO_4^{2-} should be limited to 0.6 mequiv g^{-1}, that is, less than 20% of AEC, and 2) H_2O_2 must be added in portions in such a way that the formation of the triperoxomolybdate is favored.

Experimental Section

Materials: H_2O_2 (35% in H_2O), $Mg(NO_3)_2 \cdot 6H_2O$, $Al(NO_3)_3 \cdot 9H_2O$, NaOH, and $Na_2MoO_4 \cdot 2H_2O$, purchased from Acros, Fluka, Fluka, BDH, and Aldrich, respectively, were used as such without any further purification.

Catalyst preparation: LDH preparation was based on literature procedures,[21] and is described elsewhere.[20] Starting solutions containing $Mg(NO_3)_2 \cdot 6H_2O$ (0.7 M) and $Al(NO_3)_3 \cdot 9H_2O$ (0.3 M) were mixed together slowly, while the pH wass adjusted to 10 with NaOH (1 M). For anion exchange, air-dry LDH–NO_3^- (1.5 g) was suspended in an aqueous solution (150 mL) of $Na_2MoO_4 \cdot 2H_2O$. The molybdate concentration in the exchange solution was varied to obtain compounds with different Mo loadings. Concentrations of 0.0, 1.4, 1.9, 2.7, 3.6, 4.5, 5.4, 7.5, 9.8, and 12.0 mM gave rise to samples **B**–**K**, respectively (Table 1). The anion exchange reaction ($2NO_3^- \leftrightarrow MoO_4^{2-}$) was performed under constant stirring (350 rpm) in an N_2 atmosphere (293 K) for 12 h. The final LDH–MoO_4^{2-} solid products were separated by centrifugation, washed four times with deionized water, and dried by lyophilization. Deionized and boiled water, which was cooled under an N_2 atmosphere to avoid contamination by CO_2 and irreversible anion exchange of carbonate, was used in all the synthetic procedures.

Decomposition of H_2O_2: A slurry of LDH–MoO_4^{2-} (given amount) in aqueous H_2O_2 solution (220 μL, 0.29 M) and MeOH (8 mL) was stirred magnetically at 23 ± 0.5 °C in a thermostatic bath. The evolution of the H_2O_2 concentration was followed by cerimetry.[22] Liquid samples (150 μL) were withdrawn from the slurry at regular time intervals, diluted quickly into water (15 mL), and acidified with aqueous H_2SO_4 (5 mL, 2 M). The titration was performed with aqueous $Ce(SO_4)_2 \cdot 4H_2O$ (0.1 M) by using an automatic 725 Dosimat (Metrohm).

Characterization of the LDH precursor and the Mo catalysts: For X-ray powder diffraction, a Siemens D5000*matic* with Ni-filtered $Cu_{K\alpha}$ radiation was used (40 kV, 50 mA). Cell dimensions (a_0, c_0) were calculated from the [1 1 0] and [0 0 3] reflections as reported previously.[22] IR and Raman spectra were recorded with a Nicolet FT-IR 730 and a Bruker IFS200, respectively. Raman excitation was at 1062 nm with a 50 mW Nd:YAG laser (28 scans were accumulated in 180° backscattering geometry). Brunauer–Emmet–Teller (BET) surface areas were derived from dynamic nitrogen adsorption at −196 °C by using a Coulter Omnisorp 100 CX apparatus. Before the adsorption measurements, the lyophilized samples were heated in vacuo at 125 °C for 4 h. Thermogravimetric analysis of exchanged LDH samples was performed in a Setaram TG-DTA92 balance under flowing He (20 mL min^{-1}) at a heating rate of 5 °C min^{-1}. Particle size and morphology were determined with a Philips XL30 FEG scanning electron microscope. The bulk chemical composition was determined by atomic emission spectrometry on a Varian Liberty 100 apparatus with plasma source (ICP). Samples were dissolved in HNO_3 (20%) before analysis. Electron-probe micro-analysis (EPM) was performed with a JEOL Microprobe JXA 733. ^{27}Al MAS-NMR spectra were recorded with a Bruker AMX-400 spectrometer with aqueous $Al(H_2O)_6^{3+}$ as reference.

In-situ characterization of the LDH–MoO_4^{2-} catalyst: In-situ DRS was carried out on a Varian Cary 05 UV/Vis/NIR spectrophotometer, equipped with a white-sphere accessory. Reactions were performed in a quartz cell ($1 \times 1 \times 2.5$ cm) and were started by adding aqueous H_2O_2 (53 μL of 35 wt. % solution) to a stirred suspension of **E** (0.030 g) in MeOH (2 mL) at room temperature. A suspension of **A** (0.030 g) and aqueous H_2O_2 (53 μL of 35 wt. % solution) in MeOH (2 mL) was used to obtain a baseline. The UV/Vis diffuse relectance spectra were recorded between 250 and 650 nm (40 different spectra were recorded over a 24 h period; each individual scan lasted about 6 min). In-situ FT Raman spectra were taken on a Bruker IFS200. Excitation was in the near-infrared region at 1062 nm by using a Nd:YAG laser at 200 mW. The spectra (150–4000 cm^{-1}) resulted from an accumulation of 28 scans in 180° backscattering geometry. The quartz sample cell contained MeOH (2 mL), **J** (0.2 g) corresponding to 0.17 mmol MoO_4^{2-} and H_2O_2 (300 μL, 35%).

Acknowledgements

We thank the institutions IWT (B.F.S) and FWO (D.E.D.V.) for fellowships. This work was performed in the framework of the IUAP–PAI program "Supramolecular Chemistry and Catalysis" of the Belgian Federal Government. D.E.D.V. and P.A.J. are indebted to FWO for a research grant. We thank Bart Wouters for recording the NMR spectra, and Prof. T. Zeegers-Huyskens for use of the Raman spectrometer.

[1] E. I. Spitalsky, A. Funck, *Z. Phys. Chem.* **1927**, *126*, 1.
[2] A. J. Dedman, T. J. Lewis, D. H. Richards, *J. Chem. Soc.* **1963**, 2456.
[3] J. M. Aubry, *J. Am. Chem. Soc.* **1985**, *107*, 5844.
[4] J. M. Aubry, B. Cazin, *Inorg. Chem.* **1988**, *27*, 2013.
[5] Q. J. Niu, C. S. Foote, *Inorg. Chem.* **1992**, *31,* 3472.
[6] K. Böhme, H. D. Brauer, *Inorg. Chem.* **1992**, *31*, 3468.
[7] L. J. Csányi, I. Horváth, Z. M. Galbács, '*Transition Met. Chem.* **1989**, *14*, 90.
[8] N. J. Campbell, A. C. Dengel, C. J. Edwards, W. P. Griffith, *J. Chem. Soc. Dalton Trans.* **1989**, 1203.
[9] V. Nardello, J. Marko, G. Vermeersch, J. M. Aubry, *Inorg. Chem.* **1995**, *34*, 4950.
[10] V. Nardello, S. Bouttemy, J. M. Aubry, *J. Mol. Catal. A* **1997**, *117*, 439.
[11] a) A. A. Frimer in *Singlet O_2,* CRC, Boca Raton, Florida, **1985**; b) E. L. Clennan, *Tetrahedron* **1991**, *47*, 1343; c) W. Adam, M. Prein, *Acc. Chem. Res.* **1996**, *29*, 275.
[12] a) A. U. Khan, M. Kasha, *J. Chem. Phys.* **1963**, *39*, 2105; b) C. S. Foote, *Acc. Chem. Res.* **1968**, *1*, 104.
[13] A. Gilbert, J. Baggott, in *Essentials of Molecular Photochemistry,* CRC/Blackwell, London, **1991**, p. 501.
[14] Y. Hayashi, S. Shioi, M. Togami, T. Sakan, *Chem. Lett.* **1973**, 651.
[15] J. M. Aubry, B. Cazin, F. Duprat, *J. Org. Chem.* **1989**, *54*, 726.
[16] J. M. Aubry, S. Bouttemy, *J. Am. Chem. Soc.* **1997**, *119,* 5286.
[17] S. Bouttemy, J. M. Aubry, M. Sergent, R. P. Than-Luu, *New J. Chem.* **1997**, *21*, 1073.
[18] E. C. McGoran, M. Wyborney, *Tetrahedron Lett.* **1989**, *30*, 783.
[19] F. Vanlaar, D. E. De Vos, D. L. Vanoppen, B. F. Sels, P. A. Jacobs, F. Pierard, *Chem. Commun*. **1998**, 267.
[20] B. F. Sels, D. E. De Vos, P. J. Grobet, F. Pierard, A. Kirsch-De Mesmaeker, P. A. Jacobs, *J. Phys. Chem*. *B* **1999**, *103*, 11114.
[21] F. Trifirò, A. Vaccari, *Comprehensive Supramolecular Chemistry, Vol 7* (Eds.: G. Alberti, T. Bein), Pergamon, Oxford, **1996**, pp. 251–291, and references therein.
[22] A. I. Vogel, J. Basset, *Vogel's Textbook of Quantitative Inorganic Analysis*, Longman, London, **1978**.
[23] a) S. Miyata, *Clays Clay Miner*. **1983**, *4*, 305; b) P. K. Dutta, M. Puri, *J. Phys. Chem*. **1989**, *96*, 376.
[24] F. Cavani, F. Trifirò, A. Vaccari, *Catal. Today,* **1991**, *11*, 173.
[25] S. Miyata, T. Kumura, M. Shimada, US Patent 3879525, **1975** [*Chem. Abs.* **1971**, *75*, 153442u].
[26] A. Ookubo, K. Ooi, F. Tani, H. Hayashi, *Langmuir* **1994**, *10*, 407.
[27] O. Lebedeva, D. Tichit, B. Coq, *Appl. Catal. A* **1999**, *183*, 61.
[28] For references on ^{27}Al NMR of LDH phases see: a) F. Thevenot, R. Szymanski, P. Chaumette, *Clays Clay Miner.* **1989**, *37*, 396; b) C. W. Hu, Q. L. He, Y. H. Zhang, Y. Y. Liu, Y. F. Zhang, T. D. Tang, J. Y. Zhang, E. B. Wang, *Chem. Commun*. **1996**, 121; c) C. Depège, F. Z. El Metoui, C. Forano, A. de Roy, J. Dupuis, J. P. Besse, *Chem. Mater.* **1996**, *8*, 952.
[29] K. Nakamoto, *Infrared and Raman Spectra of Inorganic and Coordination Compounds*, 5th ed., Wiley, New York, **1997**.
[30] D. L. Bish, G. W. Brindley, *Am. Mineral*. **1977**, *62,* 458.
[31] a) H. Jeziorowski, H. Knözinger, *J. Phys. Chem.* **1979**, *83*, 1166; b) J. W. Niemantsverdriet, *Spectroscopy in Catalysis*, VCH, Weinheim, **1995**.
[32] a) J. A. Connor, C. Ebsworth, *Adv. Inorg. Chem. Radiochem.* **1964**, *6*, 279; b) L. J. Csányi, *Transition Met. Chem*. **1990**, *15,* 371; c) M. H. Dickman, M. T. Pope, *Chem. Rev*. **1994**, *94*, 569.
[33] W. P. Griffith, *J. Chem. Soc.* **1963**, 5345.
[34] S. U. Kreingol'd, A. N. Vasnev, *Russ. J. Inorg. Chem. (Engl. Transl.)* **1980**, *25*, 1355.
[35] Research Information Database, Agency of Industrial Science and Technology (Japan), http://www.aist.go.jp/RIODB.
[36] a) H. C. B. Hansen, *Proc. 10th Int. Clay Conf.* **1995**, 201; b) M. Ménétrier, K. S. Han, L. Guerlou-Demourgues, C. Delmas, *Inorg. Chem*. **1997**, *36,* 2441.
[37] a) M. A. Dredzon, *Inorg. Chem.* **1988**, *27,* 4628; b) M. A. Dredzon, US Patent 4774212, **1988** [*Chem. Abs.* **1989**, *110*, 83013v]; c) M. Chibwe, W. Jones, *Chem. Mater*. **1989**, *1*, 489.
[38] V. R. L. Constantino, T. J. Pinnavaia, *Inorg. Chem*. **1995**, *34*, 883.
[39] N. I. Moiseeva, A. E. Gekhman, I. Moiseev, *J. Mol. Catal. A* **1997**, *117*, 39.
[40] D. L. Vanoppen, D. E. De Vos, P. A. Jacobs, *J. Catal*. **1998**, *177,* 22.

Received: December 11, 2000 [F2928]

